cmgh
CELLULAR AND MOLECULAR GASTROENTEROLOGY AND HEPATOLOGY

ORIGINAL RESEARCH

Novel Human NKCC1 Mutations Cause Defects in Goblet Cell Mucus Secretion and Chronic Inflammation

Rainelli Koumangoye,[1] Salma Omer,[1] Mustafa H. Kabeer,[2,3] and Eric Delpire[1]

[1]Department of Anesthesiology, Vanderbilt University School of Medicine, Nashville, Tennessee; [2]Pediatric General and Thoracic Surgery, Children's Hospital Orange County, Orange, California; [3]Department of Surgery, University of California, Irvine, California

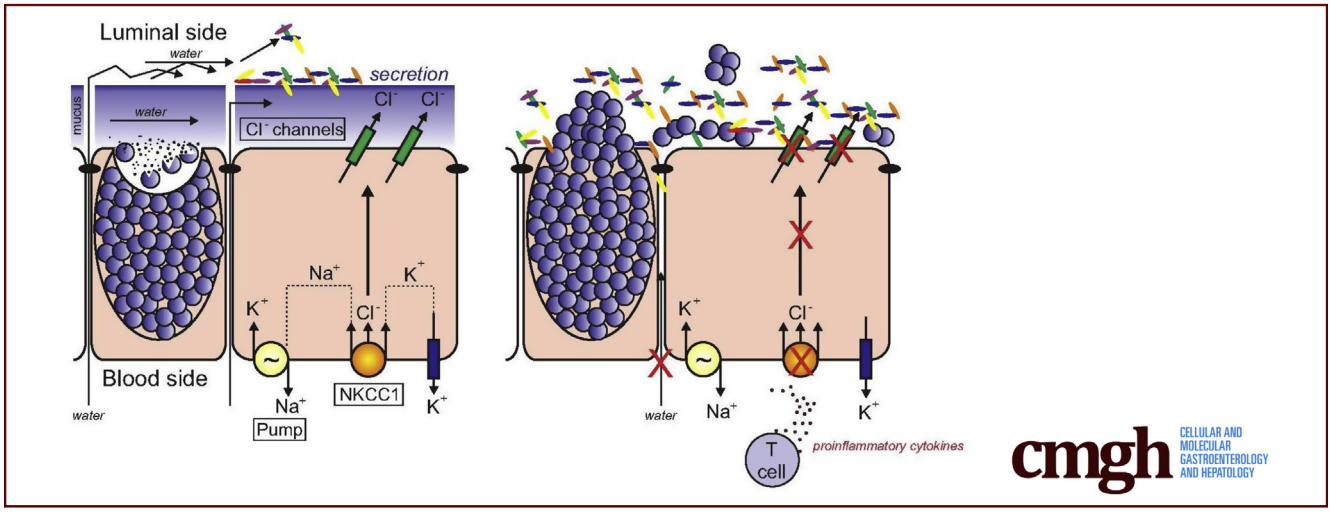

SUMMARY

A mouse model that recapitulates a unique human mutation in the Na^+-K^+-$2Cl^-$ cotransporter shows a deficit in intestinal water and mucus secretion. Abnormal hydration and mucus integrity leads to bacterial invasion of the epithelium, and reduced ability of the intestine to clear bacterial infections. The same impaired gut barrier function that we observed in the mouse likely contributed to the deficit of the gastrointestinal tract of the patient.

BACKGROUND & AIMS: Infections resulting from intestinal yeast and bacteria affect a large number of patients with deficits in absorptive or secretory epithelial transport mechanisms. The basolateral Na^+-K^+-$2Cl^-$ cotransporter (NKCC1) has been implicated in intestinal epithelial fluid secretion. Two patients with deleterious heterozygous (NKCC1-DFX, DFX for Asp-Phe-stop codon) or homozygous (Kilquist) mutations in *SLC12A2* (NKCC1) suffered from gastrointestinal deficits. Because of chronic infections, the colon and the small intestine of the NKCC1-DFX patient were resected surgically.

METHODS: To investigate how NKCC1 affects the integrity and function of the gut epithelia, we used a mouse model recapitulating the NKCC1-DFX patient mutation. Electron microscopy and immunostaining were used to analyze the integrity of the colonic mucus layers and immune cell infiltration. Fluorescence in situ hybridization was performed on the distal colon sections to measure bacteria translocation to the mucosa and submucosa. *Citrobacter rodentium* was used to measure mouse ability to clear enteric infection. A multiplex cytokine assay was used to analyze mouse inflammatory response to infection.

RESULTS: We show that NKCC1-DFX expression causes defective goblet cell mucus granule exocytosis, leading to secretion of intact granules into the lumen of the large intestine. In addition, NKCC1-DFX colon submucosal glands secrete mucus that remained attached to the epithelium. Importantly, expression of the mutant NKCC1 or complete loss of NKCC1 function leads to aggravated inflammatory response to *C rodentium* infection. Compared with wild-type, NKCC1-DFX mice showed decreased expression of claudin-2, a tight junction protein involved in paracellular Na^+ and water transport and enteric infection clearance.

CONCLUSIONS: Our data indicate that NKCC1-DFX impairs gut barrier function by affecting mucus secretion and immune properties. *(Cell Mol Gastroenterol Hepatol 2020;9:239–255; https://doi.org/10.1016/j.jcmgh.2019.10.006)*

Keywords: NKCC1; Goblet Cell; Mucus Secretion; Bacterial Infection.

The Na-K-2Cl cotransporter (NKCC1) promotes the tightly coupled movement of Na^+, K^+, and Cl^- ions[1] across the plasma membrane of many cells, including

neurons,[2–5] smooth muscle cells,[6,7] and epithelial cells.[8–12] Because of its importance in the function of so many cell types, the human Na-K-2Cl transporter likely is resistant to deleterious mutations. However, 2 patients with unique mutations in *SLC12A2* (NKCC1) recently were described and they both suffer from severe intestinal dysfunction.[13,14] In 2016, we reported the case of a 16-year-old girl who gradually lost all gastrointestinal function and now requires total parenteral nutrition.[13] She carries a de novo frameshift mutation in exon 22 of *SLC12A2*, leading to truncation of a large portion of the cytosolic carboxyl-terminal tail of the transporter. The mutation, called NKCC1-DFX, was shown to exert dominant-negative effects on the trafficking of the wild-type transporter in epithelial cells, including in a novel mouse model that recapitulates the mutation of the patient.[15] Earlier this year, the case of a 5-year-old boy with complete deletion of NKCC1 resulting from homozygous loss of exons 2–7 was reported.[14] The patient suffers from severe gastrointestinal deficits, including midgut malrotation and a mucus secretion deficit. As was the case with the first patient, his weight loss and failure to thrive necessitated the placement of a gastrostomy tube.

Several NKCC1 knockout (KO) mouse models were generated approximately 20 years ago. The 2 striking phenotypes were sensorineural deafness plus imbalance resulting from inner ear defects and male sterility owing to absence of proper sperm maturation.[16–19] In 1 model, periweaning lethality also was observed, resulting from intestinal obstruction.[17] Interestingly, this phenotype was not noted in another model in which most homozygote animals survived,[16] possibly indicating strain/background effects. Two studies also reported deficits in pacemaking currents in myenteric interstitial cells of Cajal in the intestine of NKCC1 KO mice.[20,21]

The prime function of the intestine is to absorb small nutrients derived from food broken down in the upper digestive tract. This work is performed by epithelial cells that line the inner surface of the gut. To facilitate transit, epithelial cells also modify the composition of the intestinal content, including its hydration. Along the length of the intestine, hydration of the stool is modified by water absorption and secretion. Water secretion is driven by the movement of Cl^- through apical Cl^- channel (Cystic Fibrosis Transmembrane conductance Regulator) and basolateral NKCC1.[22] As in the lung, these epithelial cells are exposed to the external milieu, including potential pathogens, and they secrete layers of mucus to protect themselves from this outside environment. Proper intestinal function also requires peristalsis or contractile movement of smooth muscle cells, a process under the control of the enteric nervous system. Thus, the work of the intestine relies on the function of many cell types that work in concert to achieve the overall mission of the tissue.

The present study was designed to understand the basis for the intestinal infection that led to colon and small intestine resection in the NKCC1-DFX patient. Our results identify deficits in stool hydration, mucus release, and mucus barrier integrity in the colon, leading to interaction of commensal bacteria with the underlying epithelium, exaggerated inflammatory response, and a reduced ability to clear bacterial infection.

Results

The purpose of this study was to understand the cellular defects that led to the total colectomy and eventual subtotal enterectomy in an undiagnosed patient carrying a de novo mutation in the gene encoding the Na-K-2Cl cotransporter, NKCC1. Pathology of the specimen showed proximal colon hyperemia and edema, with the distal portion being grossly thickened with some adherent exudative material. The midportion of the colon had some focal hyperemia. The distal 2.5 cm of small intestine included in the specimen had some soft-tissue duskiness and hyperemia. It is unclear which portions of these pathologic findings were the result of patient disease and how much of it occurred from handling the tissue during laparoscopy. It was also of interest to note that the small bowel had normal peristalsis during laparoscopy even though the patient had no clinical motility, was never able to tolerate enteral feeds, and required proximal gastric and jejunal decompression owing to a retrograde flow of bile that suggested functional obstruction but no mechanical obstruction. The colectomy and eventual enterectomy were performed out of desperation to exclude entry points of life-threatening yeast resulting in sepsis, which has significantly decreased since the surgery. The patient has been struggling with eventual liver dysfunction resulting from the short intestinal length and prolonged total parenteral nutrition, but has enjoyed a significantly enhanced quality of life.

Relationship Between Mouse Strains and the Survival of NKCC1 Knockout Mice

In addition to the patient carrying the NKCC1-DFX mutation,[13] the patient completely lacking NKCC1 expression[14] suffered from severe intestinal dysfunction. To establish the relationship between the cotransporter and intestinal function, we examined the intestine of wild-type, NKCC1-DFX heterozygote[15] and homozygote mice. Note that when original KO mice were generated and studies were published in 1999, some laboratories noticed periweaning lethality,[17] although others did not,[16] indicating a possible strain/background effect. Similarly, when we generated our NKCC1-DFX mouse line, we noticed that most of our first-generation mice (ie, those generated from direct Clustered Regularly Interspaced Short Palindromic Repeats/CRISPR

Abbreviations used in this paper: **AB/PAS, Alcian blue and periodic acid–Schiff; DAPI, 4′,6-diamidino-2-phenylindole; FITC, fluorescein isothiocyanate; IHC, immunohistochemistry; KO, knockout; LB, Luria Broth; Muc2, mucin 2; NKCC1, Na-K-2Cl cotransporter 1; PBS, phosphate-buffered saline; PCR, polymerase chain reaction; TFF3, Trefoil factor 3; TNF-α, tumor necrosis factor-α; UEA-1, *Ulex europaeus* agglutinin I; WT, wild-type.**

Most current article

2352-345X
https://doi.org/10.1016/j.jcmgh.2019.10.006

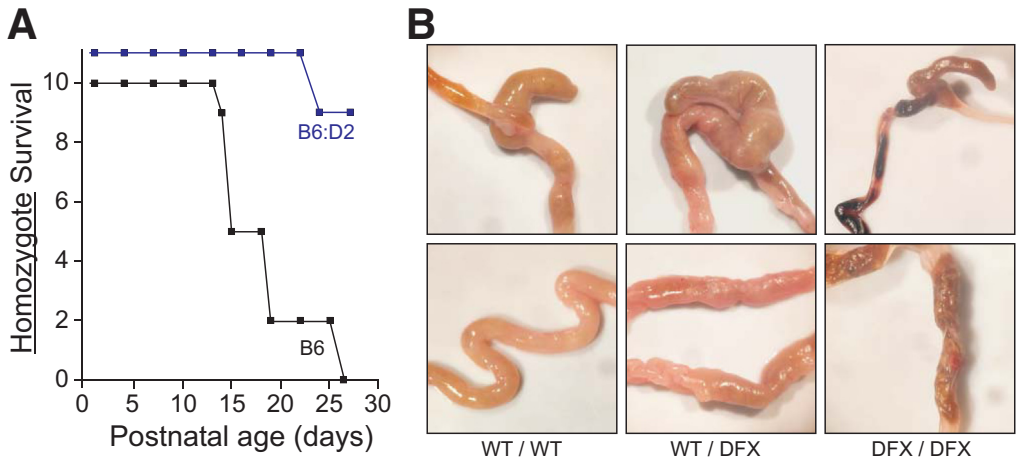

Figure 1. Deletion of NKCC1 results in death in C57BL/6J. (*A*) NKCC1DFX/DFX mice in C57BL/6J and mixed C57BL/6J:DBA/2J background were maintained in a pathogen-free environment and survival was determined. The B6:D2 KO mice that survived the periweaning period lived for several months until use. (*B*) Gross anatomy of the cecum and colon of NKCC1$^{WT/WT}$, NKCC1$^{WT/DFX}$, and NKCC1$^{DFX/DFX}$ in C57BL/6J background around weaning time.

Associated Protein 9 (CRISPR/Cas9) embryonic injection in a B6:D2 background), were viable compound heterozygous knockouts. Upon backcrossing of the DFX allele into C57BL/6J, we lost ability to produce adult homozygotes. Figure 1*A* shows survival of NKCC1$^{DFX/DFX}$ (KO) mice in C57BL6/J (>5 generations) vs a mixed B6:D2 background. An anatomic examination of the intestine in the 3 genotypes showed tissue shrinkage, especially in the NKCC1 homozygote mice (Figure 1*B*). As previously shown by Flagella,[17] blood also was observed in the intestine of NKCC1$^{DFX/DFX}$ mice.

Intestinal Transit and Feces Water Content Deficits in NKCC1-DFX and KO Mice

To assess the overall function of the intestinal tract of mice, we collected pellets from NKCC1$^{wild\text{-}type\ (WT)/WT}$, NKCC1$^{WT/DFX}$, and NKCC1$^{DFX/DFX}$ mice and determined their water content. A significant reduction in water content was observed in both NKCC1$^{WT/DFX}$ and NKCC1$^{DFX/DFX}$ mouse pellets, compared with controls, indicating a deficit in water secretion in the intestine (Figure 2*A*). Gastrointestinal transit time was measured after gavage of a carmine (bright red) dye. There was no difference between controls and NKCC1$^{WT/DFX}$ mice, but a significant delay in transit time in NKCC1$^{DFX/DFX}$ mice (Figure 2*B*). This phenotype was confirmed by killing the animals and counting the number of pellets transiting in the intestinal tract. There was a significant increase in the number of formed pellets in the colons of NKCC1$^{DFX/DFX}$ mice, compared with their wild-type and heterozygote counterparts (Figure 2*C* and *D*).

NKCC1 Is Required for Normal Goblet Cell Mucus Granule Exocytosis

Epithelial cells in the intestine separate bacteria in the lumen from the mucosal immune system and from the circulation. The first line of defense against intestinal bacteria is formed by layers of secreted mucus that protect the epithelium.[23] Sheets of mucin 2 (Muc2)-containing mucus are secreted by goblet cells. In the colon, the mucus is composed of 2 layers: an outer layer that is home to commensal bacteria, and an inner layer that is packed more densely and impenetrable to bacteria.[24] By using transmission electron microscopy, we analyzed colonic tissue isolated from NKCC1$^{WT/WT}$, NKCC1$^{WT/DFX}$, and NKCC1$^{DFX/DFX}$ mice. In WT mice, the exocrine cells containing mucin granules could be seen cupping and releasing mucus proteins into the intestinal lumen once it reached the apical surface of the intestinal epithelium (Figure 3*A* and *B*). In contrast, in NKCC1$^{WT/DFX}$ (Figure 3*C* and *D*) and NKCC1$^{DFX/DFX}$ (Figure 3*E* and *F*) mice, these cells failed to form the typical cupping shape before releasing the mucins and instead showed mucin granules abnormally plugging the apical membrane. In addition, intact mucin granules could be seen floating in the lumen (Figure 3*C* and *E*). These abnormal phenotypes were quantitated in 3 mice, with 8 sections per mouse. Of the 24 wild-type sections, none had abnormal theca release and none had intact granules observed floating in the lumen. In contrast, 7 abnormal theca releases and 2 groups of intact granules in the lumen were observed in the NKCC1-DFX sections, whereas of 24 micrographs of KO tissue, 11 had abnormal theca release and 3 micrographs showed floating granules in the lumen. A similar pattern was seen with exocrine cells located at the base of the crypt (data not shown). To confirm the presence of mucin granules in the lumen of NKCC1-DFX and NKCC1-KO mice colons, we performed immunohistochemistry (IHC) staining with a Clca1 antibody (protein also called Clca3 and gob-5). Clca1 is a chloride channel accessory protein located in the membrane of mucin granules in goblet cells of the intestinal, respiratory, and reproductive tracts.[25] In WT mice, very little to no Clca1 staining was observed in the colon lumen (Figure 3*G*). In contrast, in colon sections of NKCC1$^{WT/DFX}$ (Figure 3*H*) and NKCC1$^{DFX/DFX}$ (Figure 3*I*) mice, a strong Clca1 signal was observed in the lumen,

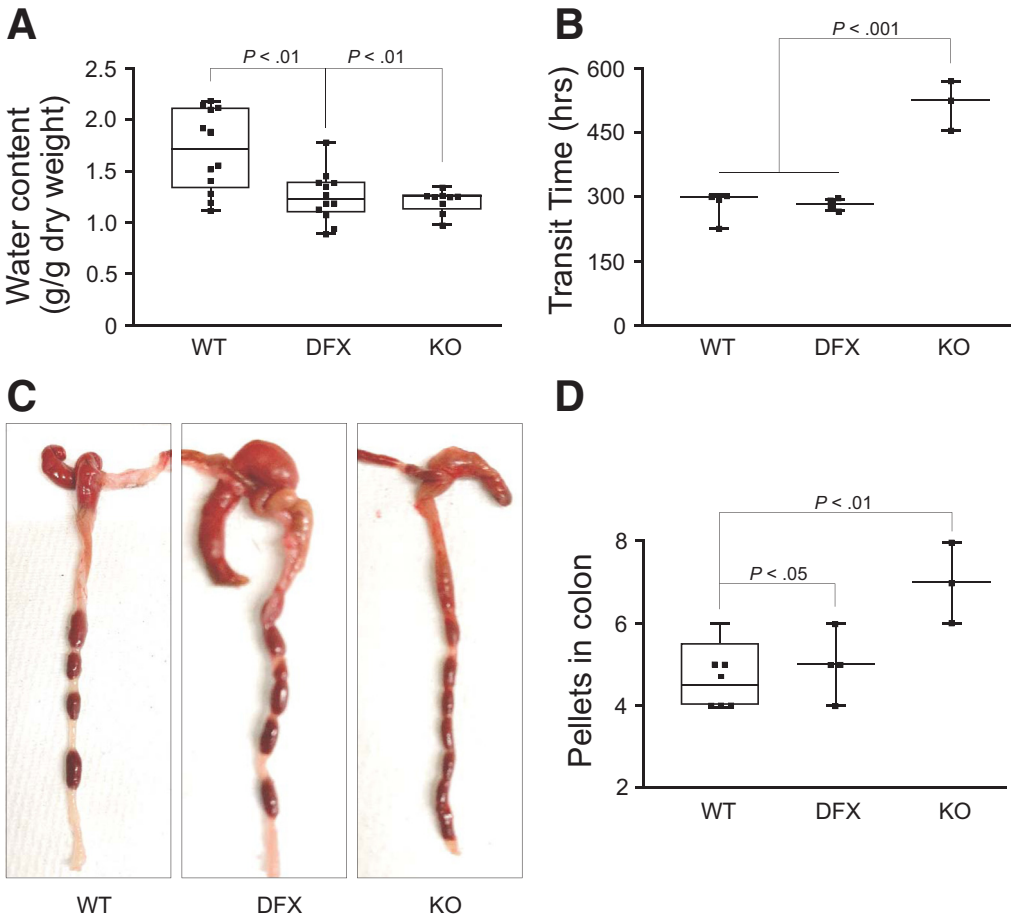

Figure 2. Abnormal water and intestinal transit are observed in NKCC1-DFX mutant mice. (*A*) Water content of fecal pellets collected from WT NKCC1$^{WT/WT}$, NKCC1$^{WT/DFX}$, and NKCC1$^{DFX/DFX}$ mice. Whisker plot data presents the median, lower and upper quartiles, and minimum and maximum for 9–12 pellets from 3–4 animals per group. (*B*) Gastrointestinal transit time measured by subtracting time of oral gavage with 6% carmine red solution from time of appearance of red fecal pellets (n = 3–4 mice per group). (*C* and *D*) The number of pellets increases in the colon of NKCC1$^{DFX/DFX}$ mice. (*A*, *B*, and *D*) *P* values were obtained from 1-way analysis of variance with follow-up Tukey posttests.

mostly sticking to the epithelial layer, indicating that Clca1 accumulates in the mucus gel of NKCC1$^{WT/DFX}$ and NKCC1$^{DFX/DFX}$ mice.

Loss of NKCC1 Function Impairs the Organization of the Outer and Inner Mucus Layers

To assess the composition and physical characteristics of the mucus layers in the colon of NKCC1$^{WT/WT}$, NKCC1$^{WT/DFX}$, and NKCC1$^{DFX/DFX}$ mice, we first stained Carnoy-fixed colon sections with Alcian blue and periodic acid–Schiff (AB/PAS) to stain polysaccharides and observed no significant difference in the number of goblet cells between the WT and NKCC1-DFX mice (Figure 4*A*, *B*, and *D*). A small but significant decrease ($P < .05$) was observed in the kO mice (Figure 4*A*, *C*, and *D*). To test whether goblet cell maturation was affected, we examined messenger RNA expression levels of key proteins involved in the differentiation and maturation process of these cells. We observed no difference in the messenger RNA expression of Hes1, Gfi1, Kif4, Spdef1, and Trefoil factor 3 (TFF3) among the 3 genotypes (Figure 4*E*–*I*). We then used IHC to examine the mucus using an anti-muc2 antibody. In contrast to WT mice in which the mucus layer separates the mucosa from stools (Figure 4*J*), in NKCC1$^{WT/DFX}$ (Figure 4*K*) and NKCC1$^{DFX/DFX}$ (Figure 4*L*) mouse sections, the mucus layer appears thinner and occasionally discontinued. A similar phenotype was observed in the colon of the affected DFX patient, but not in colon sections from healthy controls. Indeed, H&E-stained sections from the control colon shows open crypt lumens with little dense material (Figure 5*A*–*C*), whereas the section of the NKCC1-DFX patient shows plugging of materials in the crypt interior (Figure 5*D*–*F*). In addition, AB/PAS-stained sections show little signal at the surface of control colonic epithelial cells (Figure 5*G*), but clear staining at the surface of the epithelial cells in the NKCC1-DFX colon (Figure 5*H* and *I*).

To better visualize the inner and outer mucus layer in mouse colon sections, we next stained with a fluorescein isothiocyanate (FITC)-tagged *Ulex europaeus* agglutinin I (UEA-1) lectin. As seen in Figure 6, mucus layers that are nicely stratified are observed in WT sections (Figure 6*A* and *D*), whereas the number of mucin layers was reduced significantly in WT/DFX colon (Figure 6*B* and *E*), and was almost absent in the DFX/DFX colon (Figure 6*C* and *F*). We measured the thickness of the inner mucus layer and compared it with WT mice, the thickness was reduced significantly in both the WT/DFX and DFX/DFX mice (Figure 6*G*).

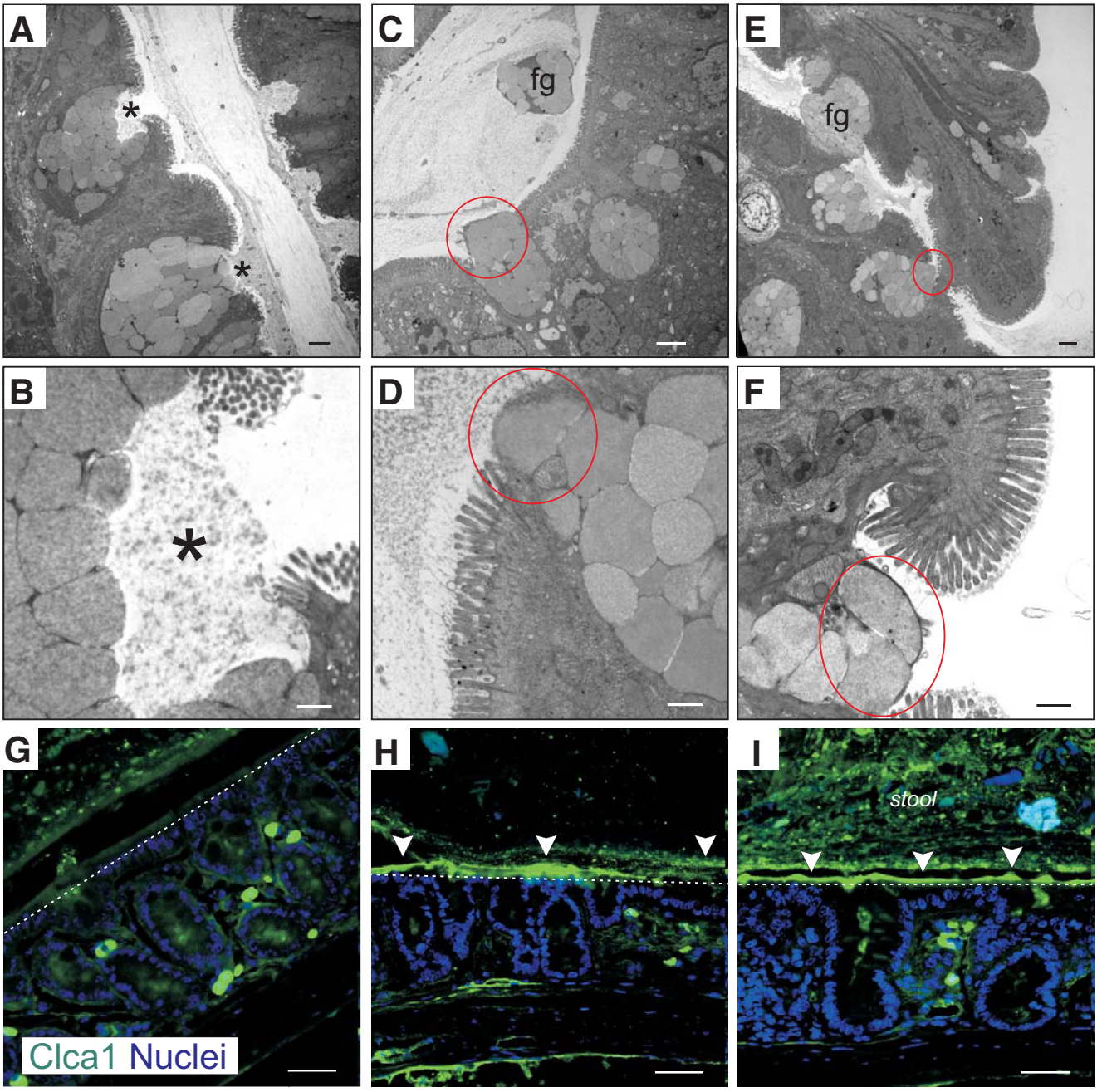

Figure 3. NKCC1 is required for goblet cells mucus granule exocytosis. Representative transmission electron microscopy images of (*A* and *B*) NKCC1$^{WT/WT}$, (*C* and *D*) NKCC1$^{WT/DFX}$, and (*E* and *F*) NKCC1$^{DFX/DFX}$ mouse colon sections. In this experiment, 3 mice per group and 10–20 micrographs per mouse section were analyzed. *Stars* show the proper release of mucus from goblet cell granules. *Red circles* highlight improper release of intact mucus granules. *Scale bars*: (*A*, *C*, and *E*) 2 μm, and (*B*, *D*, and *F*) 500 nm. (*G–I*) Representative immunostaining of mucus granules with specific protein CLCA1 (green), counterstained with DAPI (blue). *Arrowheads* indicate accumulation of CLCA1 in the lumen of NKCC1$^{WT/DFX}$ and NKCC1$^{DFX/DFX}$ mouse colons. *Dotted lines* mark the surface of the epithelium. Fg, floating granules.

Bacteria Are Found Near the Epithelium in NKCC1$^{WT/DFX}$ and NKCC1$^{DFX/DFX}$ Mice

One of the fundamental roles of the mucus layer in the intestine is to separate commensal pathogens from the epithelium and underlining immune system. To explore the consequence of defective mucus secretion, we performed fluorescence in situ hybridization in Carnoy-fixed colon sections with a Cy3-tagged EUB338 bacterial probe. The red/orange fluorescent Cy3 dye conjugated to the oligonucleotide allows for direct visualization of bacteria in tissue sections. As expected, good separation between the epithelial cells and bacteria was observed in the colon of NKCC1$^{WT/WT}$ mice (Figure 7*A*). In contrast, bacteria were detected in the

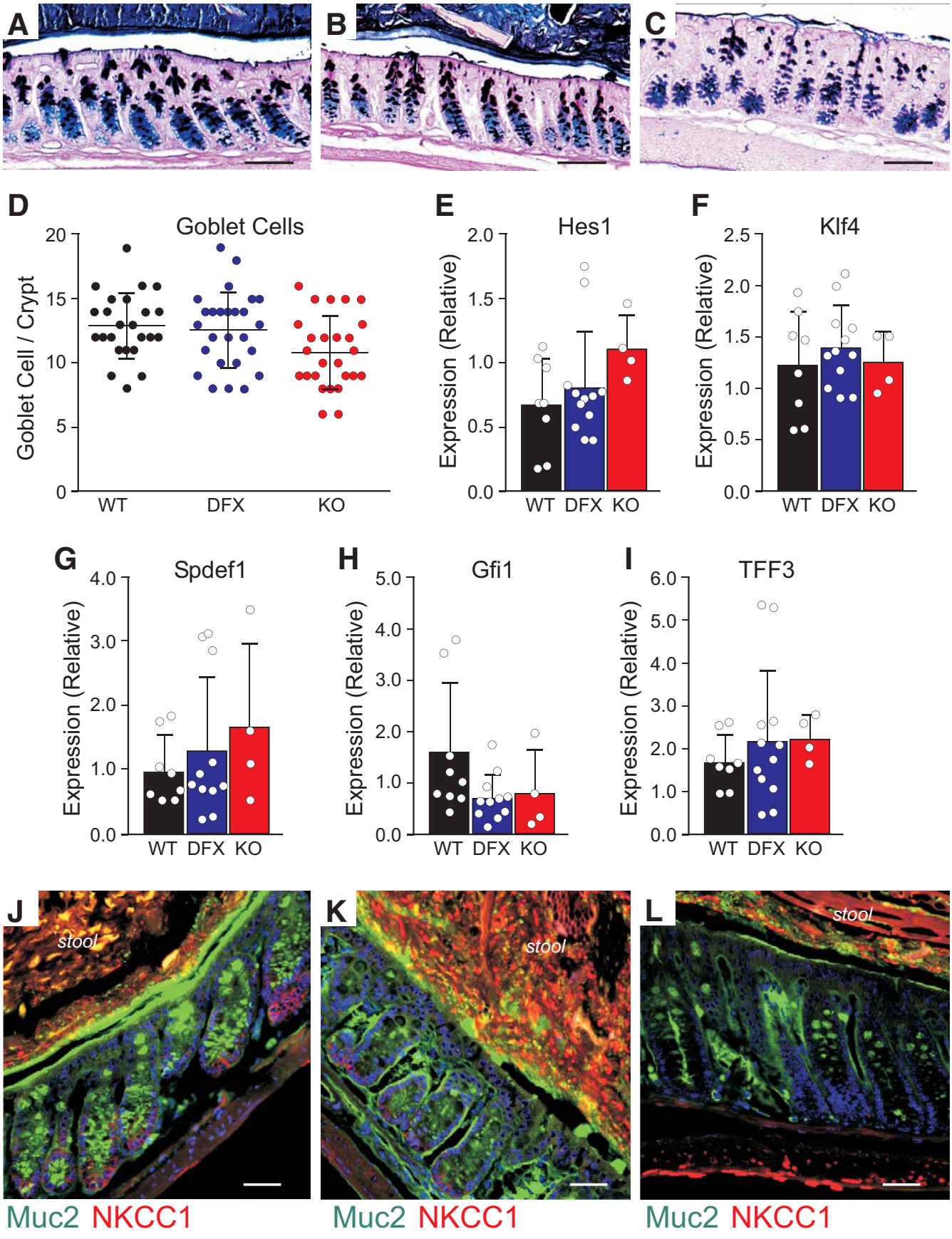
A
B
C
D
Goblet Cells
Goblet Cell / Crypt
20
15
10
5
0
WT
DFX
KO
E
Hes1
Expression (Relative)
2.0
1.5
1.0
0.5
0.0
WT DFX KO
F
Klf4
Expression (Relative)
2.5
2.0
1.5
1.0
0.5
0.0
WT DFX KO
G
Spdef1
Expression (Relative)
4.0
3.0
2.0
1.0
0.0
WT DFX KO
H
Gfi1
Expression (Relative)
5.0
4.0
3.0
2.0
1.0
0.0
WT DFX KO
I
TFF3
Expression (Relative)
6.0
5.0
4.0
3.0
2.0
1.0
0.0
WT DFX KO
J
stool
Muc2 NKCC1
K
stool
Muc2 NKCC1
L
stool
Muc2 NKCC1

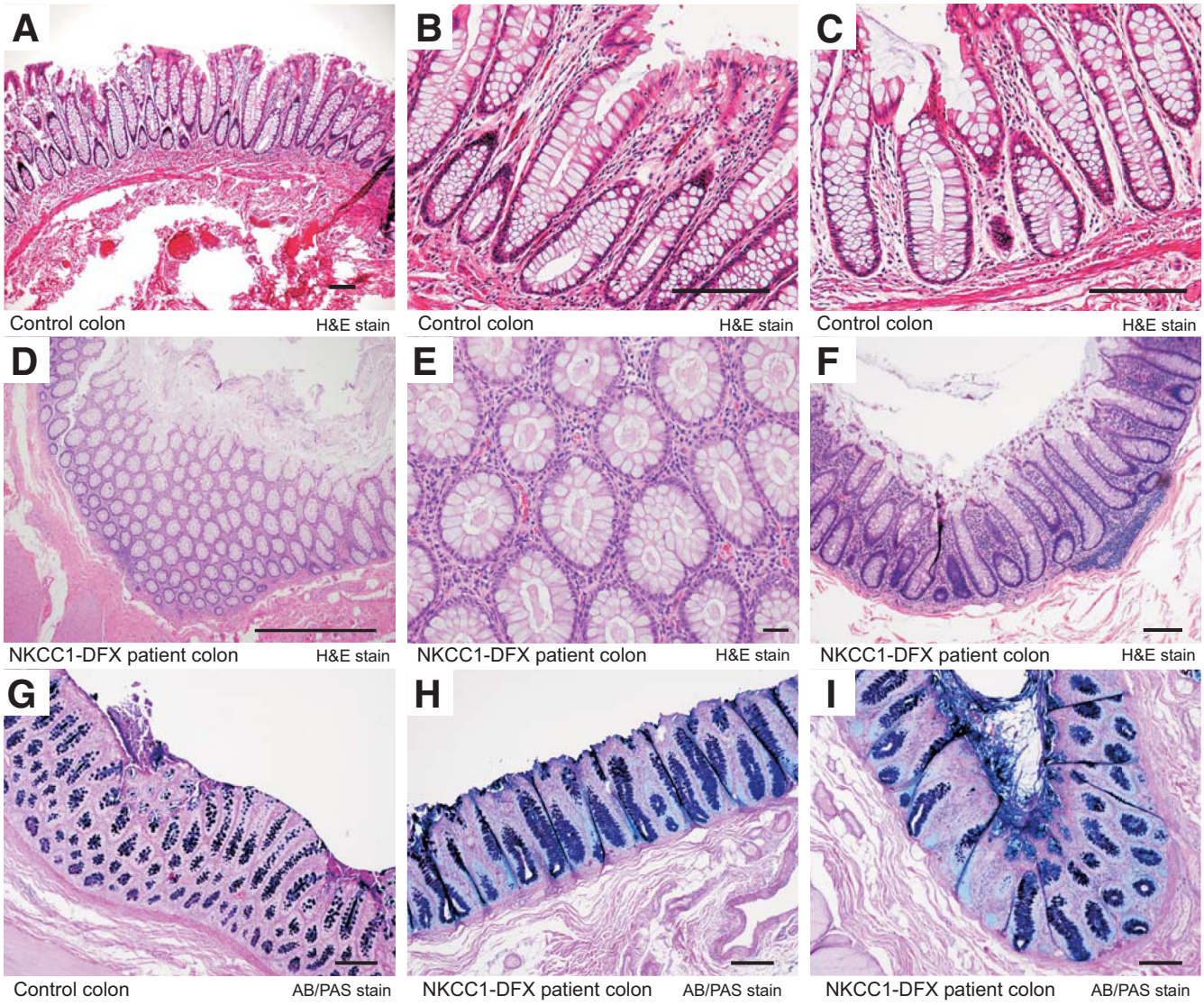

Figure 5. Evidence for mucus plugging colonic crypts in NKCC1-DFX patient. (*A–C*) H&E-stained sections of control colon showing clear crypts. (*D–F*) Evidence for dense material plugging the colonic crypts in sections of NKCC1-DFX patient. AB/PAS staining of (*G*) normal colon section and (*H* and *I*) patient colon sections showing abnormal mucus deposition at the surface of NKCC1-DFX patient colonic epithelial cells. *Scale bars*: 100 μm.

mucosa and submucosa of NKCC1$^{WT/DFX}$ (Figure 7*B*) and NKCC1$^{WT/DFX}$ (Figure 7*C*) mice. Counterstaining with FITC-conjugated UEA-1 lectin showed that bacteria infiltration occurs at segments where the inner and outer mucus layers are not formed properly (Figure 7*E* and *F*). The number of bacteria in the mucosa and submucosa was quantitated, and the numbers were significantly higher in NKCC1$^{WT/DFX}$ and NKCC1$^{DFX/DFX}$ colon sections, compared with NKCC1$^{WT/WT}$ mice (Figure 7*G*). In contrast to wild-type (Figure 7*H*), bacteria were noticed inside and close to epithelial cells in NKCC1$^{WT/DFX}$ (Figure 7*I*) and NKCC1$^{DFX/DFX}$ (Figure 7*J*).

Figure 4. (***See previous page***). **Mucus remains attached on the luminal side of the colon in both NKCC1-DFX mutant mice and the NKCC1-DFX patient.** (*A–C*) Representative AB/PAS staining of NKCC1$^{WT/WT}$, NKCC1$^{WT/DFX}$, and NKCC1$^{DFX/DFX}$ colon sections. (*D*) Quantitation of the number of PAS-positive goblet cells per crypt in intestinal sections (3 mice, 8 micrographs per mouse). One-way analysis of variance showed no significant differences between WT and DFX ($P = .092$) and between DFX and KO ($P = .066$), but a small difference between WT and KO ($P = .029$). (*E–I*) messenger RNA expression of Hes1, Klf4, Spdef1, Gfi1, and TFF3 quantitated by quantitative PCR is compared among genotypes. There were no differences between groups ($P > .05$). (*J–L*) Representative immunostaining of NKCC1$^{WT/WT}$, NKCC1$^{WT/DFX}$, and NKCC1$^{DFX/DFX}$ mouse colon sections with anti-Muc2 and anti-NKCC1 antibodies. *Scale bars*: 20 μm.

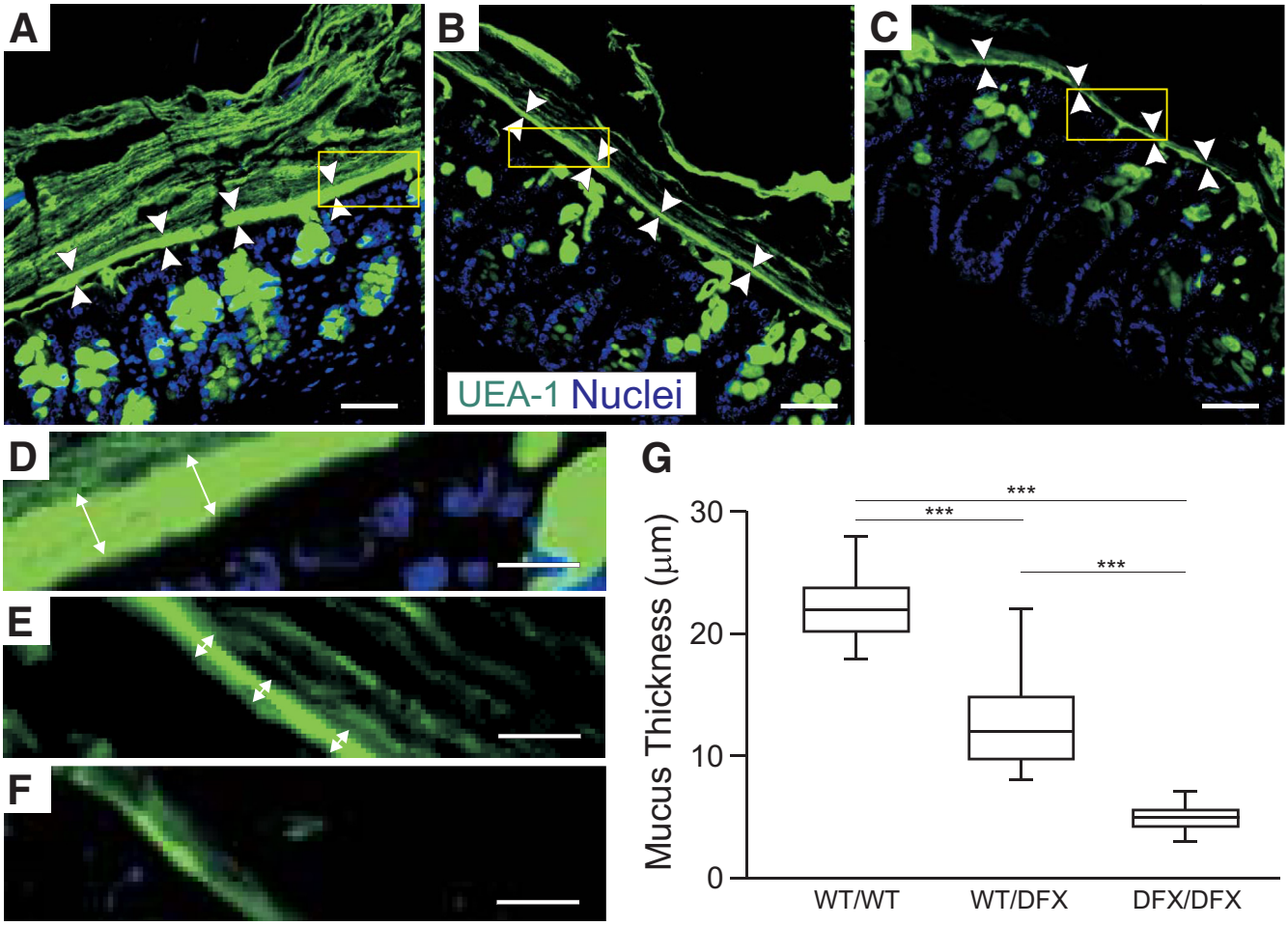

Figure 6. Loss of NKCC1 function impairs the organization of the outer and inner mucus layers. (*A–C*) UEA-1 lectin staining of colon section from (*A* and *D*) WT, (*B* and *E*) heterozygous, and (*C* and *F*) homozygous NKCC1-DFX mice. The inner mucus layer is thinner in the NKCC1$^{WT/DFX}$ and NKCC1$^{DFX/DFX}$ mice. *Scale bars*: 20 μm. (*D–F*) High magnification from indicated regions of panels *A–C*, respectively. (*G*) Quantification of the inner mucus layer thickness in the distal colon (n = 3 mice per group, 8 micrographs per mouse section). Data are shown as *whisker boxes* and statistical significance was calculated by 1-way analysis of variance followed by Tukey posttests. ***$P < .001$.

The Presence of Commensal Bacteria Might Cause Low Spontaneous Inflammation

To determine if loss of NKCC1 function affects the intestinal inflammatory response, we examined H&E colon sections of NKCC1$^{WT/WT}$, NKCC1$^{WT/DFX}$, and NKCC1$^{DFX/DFX}$ mice and looked for obvious signs of immune cell localization. No overt inflammation was noted (Figure 8*A–C*). However, IHC analysis of CD3+ cells showed a small but significant increase in CD3+ lymphocyte in NKCC1$^{DFX/DFX}$ mice (Figure 8*D–G*). Note that this was not observed all along the length of the intestinal tract but localized in isolated regions of the intestine.

NKCC1 Protects Against Enteric Citrobacter rodentium *Infection*

The presence of native bacteria within the epithelial layer of mice carrying the NKCC1-DFX allele raises the possibility that colonization might increase during enteric infection. This was investigated by testing the ability of mice to clear a *C rodentium* infection. The mouse pathogen was obtained from the American Type Culture Collection (Manassas, VA) and transfected with a vector that confers kanamycin resistance. After gavage of 2×10^9 colony forming units in 200 uL phosphate-buffered saline (PBS), fecal pellets were collected after 4 hours and after 1–9 days, gently homogenized in PBS, and aliquots plated on kanamycin plates. As seen in Figure 9, after 2 days, 50% of wild-type mice already had cleared the infection, whereas colonization was evident in DFX heterozygote and homozygote mice because pellets still contained bacteria after 9 days in 50% and 100% of mice, respectively. Inflammatory cytokines were measured in the blood of animals after 9 days postinfection. Interferon-γ and tumor necrosis factor-α (TNF-α) were detected in the plasma of NKCC1$^{DFX/DFX}$ mice (Figure 9*C*).

Claudin-2 Expression Is Limited to the Base of the Crypts in NKCC1$^{WT/DFX}$ and NKCC1$^{DFX/DFX}$ Mice

As shown in Figure 2*A*, the fecal content of NKCC1$^{WT/DFX}$ and NKCC1$^{DFX/DFX}$ mice was significantly drier than that of

wild-type mice. Transport of water to the lumen of the colon (ie, diarrhea) is an essential defense mechanism against enteric pathogens. IHC analysis showed that in WT mice claudin-2 is expressed in most cells along the length of the colonic crypts (Figure 10*A* and *B*). In contrast, claudin-2 expression was restricted to the base of the crypts in NKCC1$^{WT/DFX}$ and NKCC1$^{DFX/DFX}$ (Figure 10*B* and *C* vs *A*). The number of cells showing claudin-2 expression was reduced in both NKCC1-DFX and NKCC1-KO sections (Figure 10*D*). This observation is consistent with a deficit in transepithelial water secretion, which is needed to drive the mucus and other antibacterial peptides to the lumen of the colon. In contrast, the lateral staining of claudin-1 at the tip of the crypts was not affected by the cotransporter mutation (Figure 10*E*–*G*).

Discussion

At the start of our study, the cellular and molecular mechanisms underlying the role of NKCC1 in the intestinal pathology were unclear. In part, this is because the transporter is expressed in many cell types involved in intestinal function. By using a mouse model that recapitulates the patient mutation, we closely examined the intestinal epithelium of control mice and mice carrying 1 and 2 copies of the mutant allele. Our study provides important new information regarding the role of NKCC1 in preventing bacterial infection and inflammation in the intestine.

Our results show that the absence of NKCC1 function leads to intestinal hyperemia, a phenotype observed in young weanlings. The severity of this phenotype seems to be strain-dependent because most mice of a mixed C57BL/6J:DBA/2J background survive to adulthood, whereas mice in purer C57BL6/J background die before or shortly after weaning. The time of death likely is related to the transition from mother's milk to solid food. We noted that the loss of weanlings was observed previously in a group of NKCC1 KO animals,[17] but not in another group.[16]

We also noticed differences in the overall appearance of the colon (as shown in Figure 1*B*), with increasing signs of tissue dehydration from NKCC1$^{WT/WT}$ to NKCC1$^{WT/DFX}$, and NKCC1$^{DFX/DFX}$ colon. A smaller-diameter colon also was noted in the pathology report of the Undiagnosed Diseases Program patient 2780 (UDP-2780). This phenotype was not unexpected because NKCC1 is involved in a regulatory volume increase after a hypertonic shock in many cells[26] and because shrinkage was observed in other tissues (eg, choroid plexus) in the absence of NKCC1 function.[27,28]

The first major epithelial deficit found in these studies relates to mucus secretion. Goblet cells are the cells in the intestine that secrete gel-forming mucins. The mucus in the intestine is made from Muc2 sheets secreted by goblet cells, specialized columnar epithelial cells scattered among the lining of the intestinal epithelium. In the colon, the mucus is composed of 2 layers, the outer layer, which is home to commensal bacteria, and the inner layer, which is densely packed and impenetrable to bacteria.[24] The secretory granules containing the mucus are normally accumulated as an apical mass limited by a dense, cup-shaped layer of cytoplasm called the *theca*. For secretion, vesicles fuse and empty their content in the lumen. In both the NKCC1$^{WT/DFX}$ and NKCC1$^{DFX/DFX}$ mice, intact granules are expulsed from the theca and many are localized ectopically in the lumen at the apical membrane of epithelial cells. In addition, entire collections of granules from 1 goblet cell can be seen floating intact in the lumen. Further analysis indicated that in the mutant mice, the lumen of crypts also was packed with intact mucin granules, a phenotype that was not observed in WT mice. Our labeling of sections with CLCA1, a protein located in the mucin granule membranes of intestinal goblet cells[25] and that is normally dissolved in the mucus gel, and with Muc2 antibodies suggested abnormal biochemical properties or viscosity of the mucus NKCC1$^{WT/DFX}$ and NKCC1$^{DFX/DFX}$ mice. Intact mucus granules in the colon also could be seen in the colon crypts of NKCC1$^{DFX/DFX}$ mice, potentially creating mucus plugs.

A possible reason for a deficit in mucus secretion and a thinner mucus layer could be a defect in the formation of goblet cells. Although we detected a small decrease in the number of goblet cells in the knockout animals by PAS staining, no difference was observed in the NKCC1-DFX intestine, which also shows a thinner inner mucus layer. In addition, expression levels of markers of goblet cell maturation and differentiation were similar among all 3 genotypes. This was the case for the transcription factors Hes1, Gfi1, Kif4, and Spdef1,[29] as well as for the Muc2-associated TFF3.[30] Thus, it seems that the signaling pathways that control goblet cell differentiation in the intestine are normal in both NKCC1-DFX and NKCC1 KO mice, making it unlikely that the mucus thinning is caused by a deficit in goblet cell number. Because of the role of NKCC1 in Cl^- and HCO_3^- secretion,[31] it is far more likely that the thinner mucus layer is caused by impaired mucus expansion. Indeed, in airway epithelial cells bathed in a HCO_3^--free saline, it was shown that application of bumetanide led to the production of strands of mucus that were abnormally viscous.[32]

A major cause of microbiome imbalance and ensuing inflammation in the intestine is enteric infection. Secretion and biochemical properties of mucus are equally important factors in host defense against multiple enteric pathogen infections. Muc2 KO mice have bacteria in direct contact with the epithelium and spontaneously develop colitis.[24,33] In cystic fibrosis, the loss of CFTR-mediated chloride and bicarbonate transport results in a viscid mucus (mucoviscidosis) in most organs, leading to chronic inflammation in the airway and intestine.[34,35] Our data with NKCC1-DFX and NKCC1 KO mice show reduced thickness of the mucus inner layer and the presence of bacteria within the epithelial layer. In agreement with the observation of bacterial infiltration, we observed an increase in CD3+ lymphocyte infiltration in the epithelium. Because the pathology of the colon in UDP-2780 was not uniform, it is important to stress that in the NKCC1$^{DFX/DFX}$ mice, the thinner inner mucus layer occasionally was discontinuous, and lymphocytes and hyperemia tended to be observed focally. Based on these observations it stands to reason that in the C57BL6/J background, mice in the periweaning period likely die from

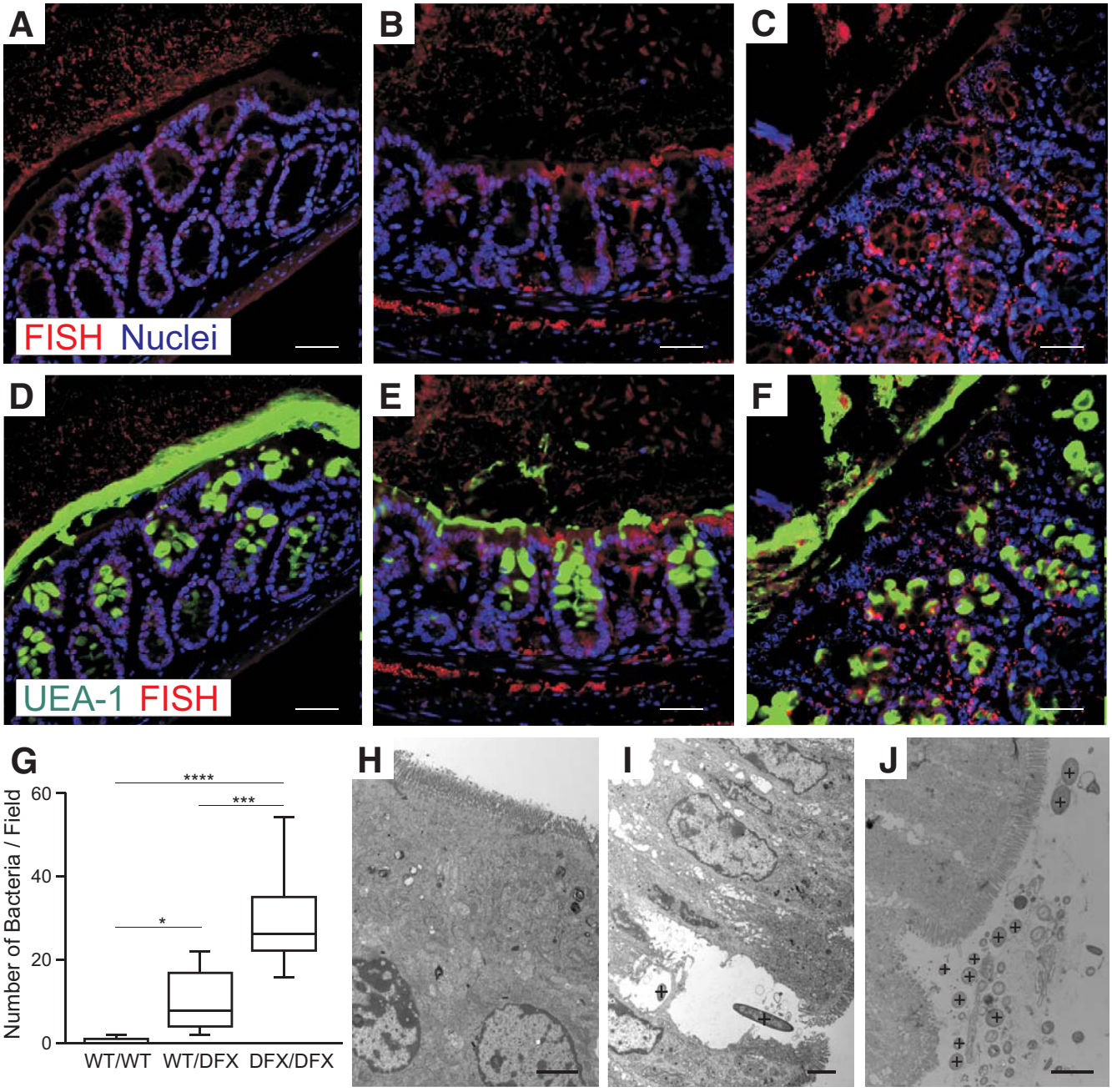

Figure 7. Bacteria penetrate the inner mucus layer in NKCC1$^{WT/DFX}$ and NKCC1$^{DFX/DFX}$ mice. Fluorescence in situ hybridization (FISH) analysis using the general bacterial probe EUB338-Cy3 (red) on (*A*) NKCC1$^{WT/WT}$, (*B*) NKCC1$^{WT/DFX}$, and (*C*) NKCC1$^{DFX/DFX}$ mouse colon sections. (*D–F*) The micrographs were counterstained with UEA-1 lectin (green) (n = 3 mice per group, 10–20 micrographs per mouse section). *Scale bars*: 20 μm. (*G*) Average number of bacteria per field in NKCC1$^{WT/WT}$, NKCC1$^{WT/DFX}$, and NKCC1$^{DFX/DFX}$ mouse colon sections (n = 3 mice per genotype, 8–12 micrographs per mouse section were counted). *$P < .01$, ***$P < .001$, and ****$P < .0001$; 1-way analysis of variance followed by Tukey posttests. (*H–J*) Electron micrographs of extensively washed colon from NKCC1$^{WT/WT}$, NKCC1$^{WT/DFX}$, and NKCC1$^{DFX/DFX}$ mice show bacteria (indicated by + signs) near the epithelium in mutant mice. *Scale bars*: 2 μm.

severe inflammatory response owing to infection in the intestine.

The fact that commensal bacteria were observed sticking to the intestinal lining of NKCC1 mutant mice predicts that upon challenge, these mice might be at increased risk to develop long-lasting infections. In fact, this is exactly what we observed after infecting mice with the *C rodentium* mouse pathogen: there was a clear genotype dependency in the ability of the intestine to clear the infection. Indeed, wild-type mice and, to a lesser extent, NKCC1$^{WT/DFX}$ mice were able to clear the infection within a few days, whereas kanamycin-resistant bacteria lingered for a significantly

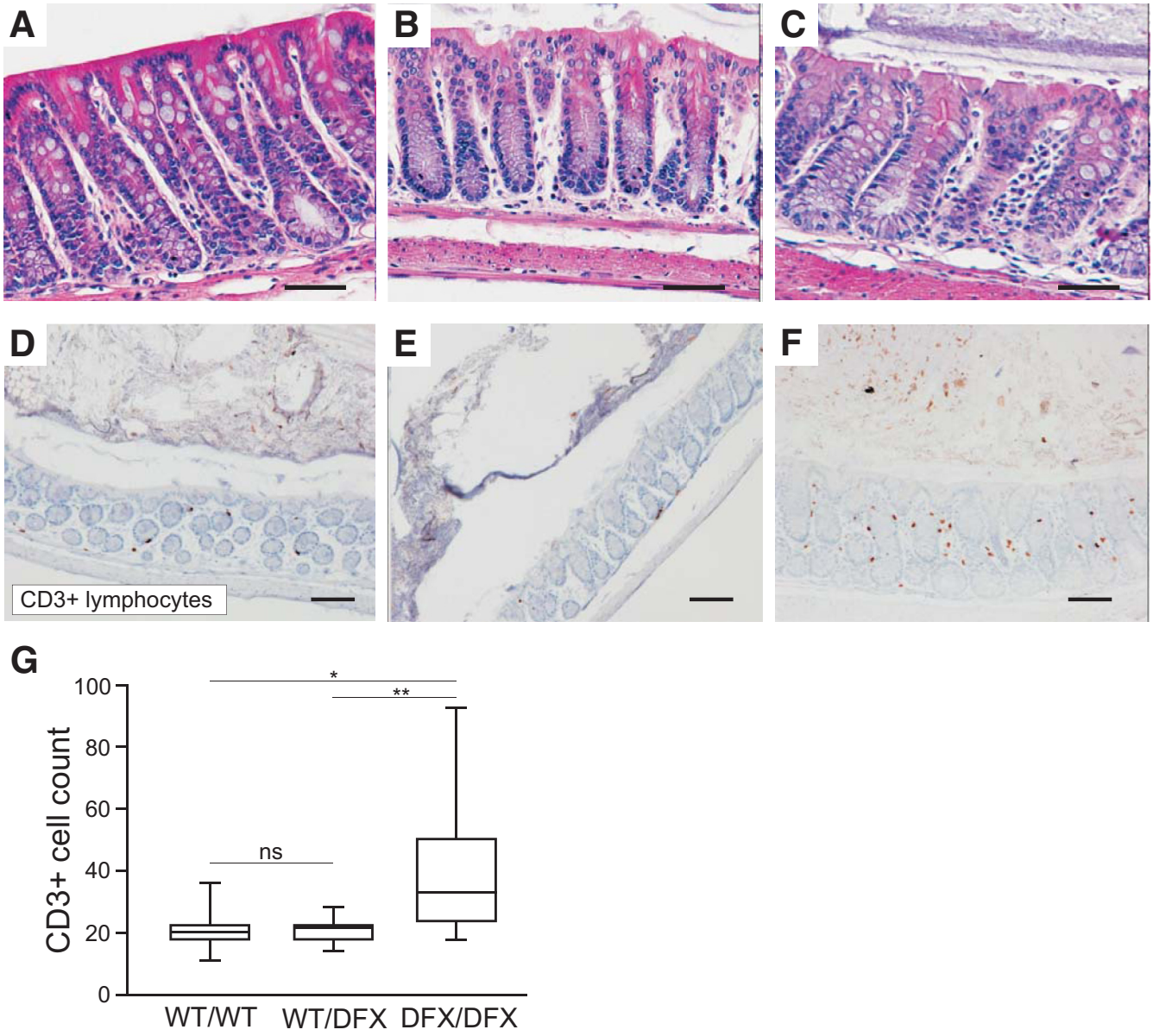

Figure 8. Loss of NKCC1 function increases CD3+ lymphocytes infiltration in the colon. (*A–C*) Representative H&E-stained micrographs of colon sections from 8-week-old NKCC1-WT, NKCC1-DFX, and NKCC1-KO mouse colon sections showing overall normal anatomy. (*D–G*) Sections of same genotypes stained with anti-CD3 antibody. *Scale bars*: 20 μm. (*G*) Quantification of the number of infiltrating CD3+ cells per genotype (N = 3 mice per group; 8 micrographs per section were taken and counted). Data are shown as *whisker box plots*, and statistical significance was calculated by 1-way analysis of variance followed by Tukey posttests. $^{*}P < .05$, $^{**}P < .01$.

longer time in the intestines of NKCC1$^{DFX/DFX}$ mice. Correlated with this lingering infection was the increased production of interferon γ and TNF-α in the blood of NKCC1$^{DFX/DFX}$ mice. The fact that TNF-α is not detectable in the serum of the DFX mice 9 days after inoculation may indicate that the course of *C rodentium* infection in the mixed-background C57:DBA mice is much faster than in a C57 background. This may explain why the WT mice clear the infection in just 9 days, as opposed to the typical 21 days that was reported previously.[36] These 2 inflammatory cytokines have been shown to contribute to the host defense during bacterial infection. In addition, TNF-α play a critical role in the early phase of inflammation by activating other proinflammatory cytokines, however, persistent TNF-α production also has been linked to chronic inflammation.[37–39] Many anti–TNF-α therapies have been developed over the past 20 years. They routinely are used to treat rheumatoid arthritis as well as other inflammatory diseases such as Crohn's disease and ulcerative colitis.[40–42]

The role of NKCC1 in the pathology likely is complex, but in part could be intimated from our observation that the water content of fecal pellets is reduced significantly in the

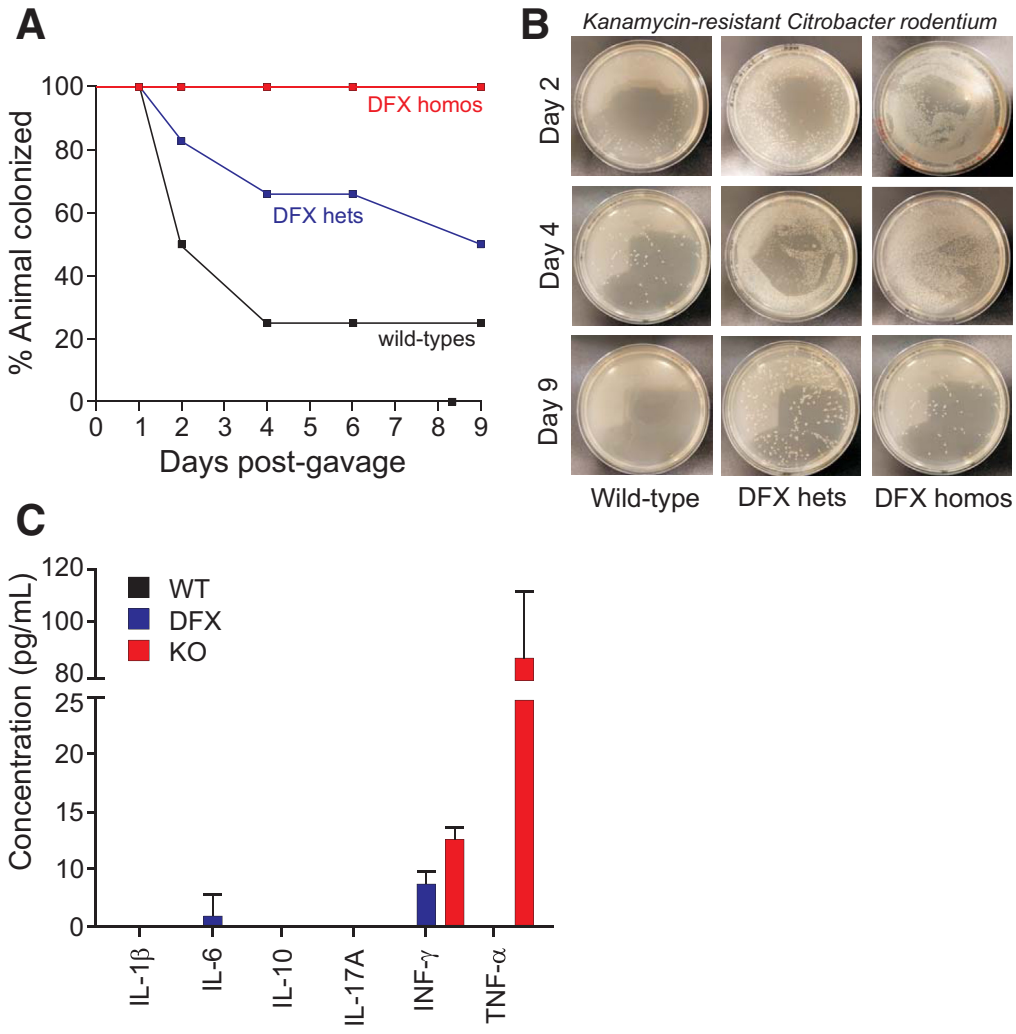

Figure 9. NKCC1 is required for enteric *C rodentium* infection clearance. $NKCC1^{WT/WT}$, $NKCC1^{WT/DFX}$, and $NKCC1^{DFX/DFX}$ mice were infected with 10^9 colony forming units of a kanamycin-resistant strain of *C rodentium*. Feces were collected every day, eluted, plated, and bacteria were enumerated. (*A*) Percentage of $NKCC1^{WT/WT}$, $NKCC1^{WT/DFX}$, and $NKCC1^{DFX/DFX}$ mice with positive *C rodentium* shedding in feces over the 9-day period. (*B*) Bacteria plated on a kanamycin-containing plate show colonization or delay clearance in $NKCC1^{WT/DFX}$ and $NKCC1^{DFX/DFX}$ mice. (*C*) Inflammatory cytokine production in the serum of $NKCC1^{WT/WT}$, $NKCC1^{WT/DFX}$, and $NKKCC1^{DFX/DFX}$ mice after 9 days postinfection (n = 3–5 mice per group, the experiment was repeated twice). hets, heterozygotes; homos, homozygotes; IL, interleukin; INF, interferon.

$NKCC1^{WT/DFX}$ and $NKCC1^{DFX/DFX}$ mice. It is well known that NKCC1 in the intestine is located on the basolateral membrane of epithelial cells. Proper NKCC1 function is critical to replenish intracellular Cl^- because the anion is secreted to the lumen by apical Cl^- channels. This Cl^- secretion leads to an electronegative lumen that drives Na^+ and water movement through paracellular pathways. Transport of water to the lumen of the gut (ie, diarrhea) is an essential defense mechanism against enteric pathogens. Thus, a deficit in mucus secretion and in transepithelial water movement is likely to account for the intestinal deficit caused by loss of NKCC1 function.

One additional supportive piece of evidence to tie the deficit to water movement in the NKCC1 mutant mice is the observation of redistribution of claudin-2 protein from the entire length of the crypt to the base only. Claudin-2 is a tight junction protein part of the paracellular barrier facilitating the movement of Na^+ ions and water molecules through the intercellular space between the epithelial cells.[43] Decrease in claudin-2 expression in the intestine was shown in Ste20-like proline/alanine-rich kinase knockout mice[44] (ie, mice lacking the terminal kinase that phosphorylate and activates NKCC1).[45] In kidney proximal tubule, deletion of claudin-2 results in a 30% decrease in fluid reabsorption.[46] Absence of claudin-2 also results in a 50% reduction in bile flow in the liver.[47] Finally, claudin-2 is upregulated in mice infected with *C rodentium*, thereby inducing diarrhea and facilitating the clearance of bacteria during infection.[48] Thus, the changes in claudin-2 localization that we observed in the distal colon of NKCC1 mutant mice are additional evidence that the cotransporter is involved in fluid secretion.

In addition to the epithelial deficit discussed here, we show that $NKCC1^{DFX/DFX}$ mice also have a deficit in intestinal transit time. In contrast to the mucus and hydration phenotypes observed in $NKCC1^{WT/DFX}$ and $NKCC1^{DFX/DFX}$ mice, the intestinal transit phenotype was observed only in the knockout animals. This phenotype likely is owing to a deficit in the pacemaking currents generated by the myenteric interstitial cells of Cajal, which lead to the contractions of the smooth muscle cell layer lining the intestinal epithelium.[20,21] In $NKCC1^{WT/DFX}$ myenteric neurons, a

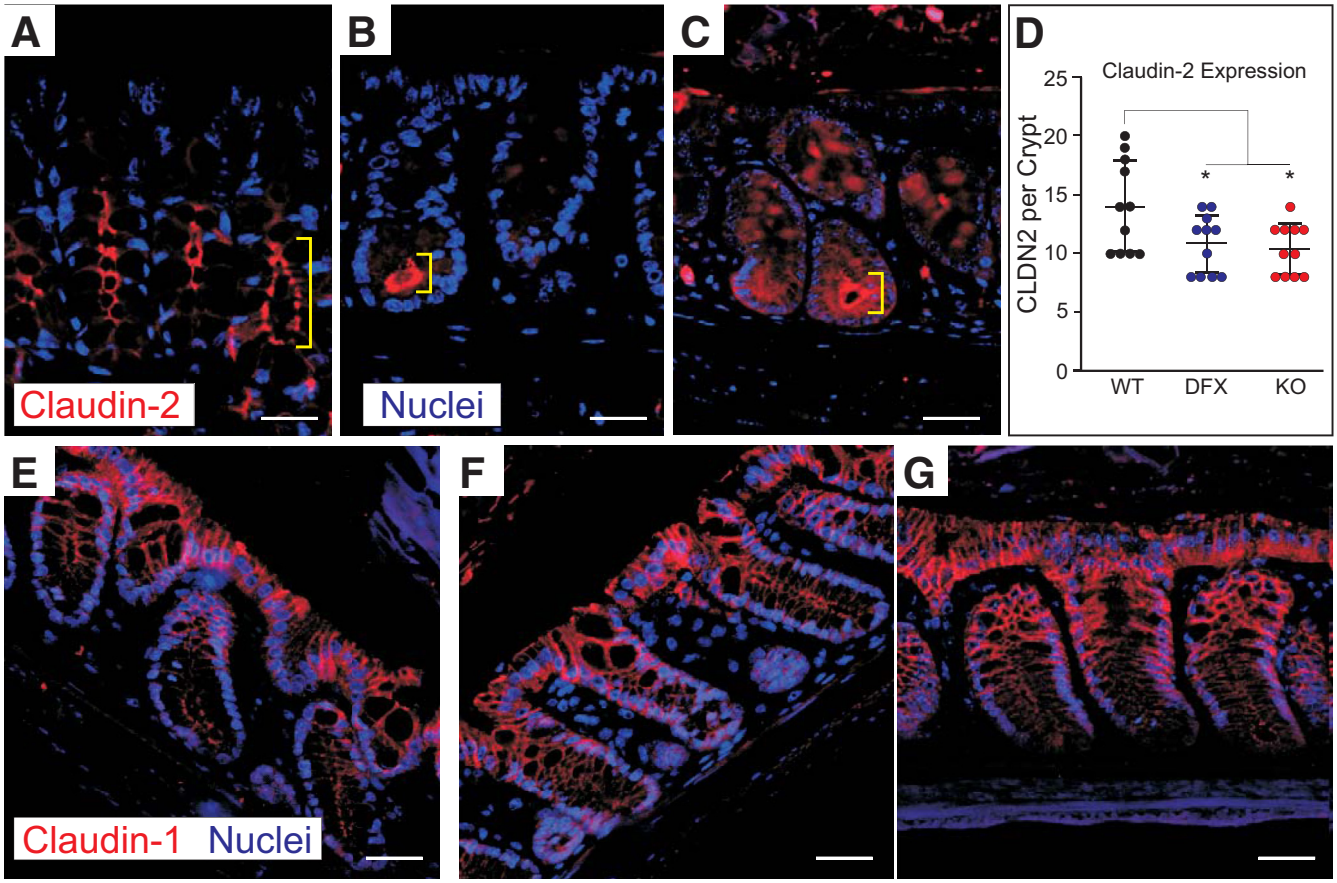

Figure 10. Claudin-2 expression is limited to the base colon of crypt in NKCC1$^{WT/DFX}$ and NKCC1$^{DFX/DFX}$ mice. Representative IF images of NKCC1$^{WT/WT}$, NKCC1$^{WT/DFX}$, and NKCC1$^{DFX/DFX}$ mouse colon sections stained with (*A–C*) claudin-2 and (*D–F*) claudin-1 antibodies (red). Sections also show DAPI (blue) or nuclei staining. (*D–F*) In contrast, claudin-1 expression at the lateral membrane was similar in all 3 genotypes. *Scale bars*: 20 μm. Number of claudin-2–positive cells per crypt were counted on 5 fields, 11 crypts per genotype. There was a significant decrease in the number of cells expressing claudin-2 in the mutant mice. $P = .043$ for NKCC1–DFX and $P = .019$ for KO. There was no difference between NKCC1-DFX and NKCC1 KO mice ($P = .93$). (*G*) Data are shown as *whisker boxes* and statistical significance was calculated by 1-way analysis of variance followed by Tukey posttests. CLDN2, claudin-2.

reduced (50%) NKCC1 expression is likely to be sufficient to sustain their pacemaking activity. This is in contrast to the dominant-negative effect that the mutant cotransporter exerts in epithelial cells.[15] We anticipate that disruption in pacemaking currents is likely to aggravate the intestinal function in the 5-year old NKCC1 knockout patient.

In summary, our studies show that the patient truncation mutation in NKCC1 is sufficient to affect mucus release and the mucus barrier that keeps bacteria from interacting with the epithelium. In combination with decreased hydration of fecal content and possibly decreased peristalsis, the bacteria at the epithelium might focally trigger inflammatory responses drawing extra blood to the tissue. The phenotype is stronger in mice with 2 copies of the nonfunctional transporter that more closely resembles the Kilquist patient. Homozygous mice in a pure C57BL/6J background are highly susceptible and develop this pathology around weaning time, leading to death. In contrast, mice of a mixed background are less susceptible, show a less severe pathology, and survive to adulthood.

Materials and Methods

Reagents

Prolong Gold antifade with 4′,6-diamidino-2-phenylindole (DAPI) was obtained from Life Technologies (Grand Island, NY). FITC-tagged UEA-1 lectin was obtained from Sigma, St. Louis, MO (cat. L9006; 10 μg/mL). The following antibodies were used as primary antibodies: NKCC1 (cat. ab59791, 1:200; Abcam); CLCA1 (Developmental Studies Hybridoma Bank 10.1.1 monoclonal, 1:100); mucin 2 (cat. sc-7314; 1:100; Santa Cruz Biotechnology, Dallas, TX); claudin-1 (cat. 71-7800, 1:200; ThermoFisher, Waltham, MA); claudin-2 (cat. 35-5600, 1:200; ThermoFisher); and Bio-Plex Pro Mouse Cytokine kit (cat. M6000007NY; Bio-Rad, Hercules, CA).

Immunohistochemistry

Segments of the distal colon (without washing) isolated from 8- to 12-week-old animals were fixed for 4 hours in Carnoy's fixative (60 mL methanol, 30 mL

chloroform, 10 mL acetic acid glacial) and embedded in paraffin. Paraffin-embedded sections were dewaxed with CitriSolv (Thermo Fisher Scientific) and were rehydrated by 3 consecutive 5-minute washes in 100%, 95%, and 70% ethanol; followed by an additional 5-minute wash in PBS. Antigens were retrieved by CitraPlus (BioGenex, Fremont, CA). Next, sections were treated with blocking buffer (5% bovine serum albumin + 1% goat serum + 0.5% Triton X-100, Sigma) in PBS for 2 hours. Sections then were stained with H&E, UEA-1 lectin, AB/PAS, or with anti-Muc2, CLND2, NKCC1, and CLCA1 antibodies. Indicated primary antibodies were resuspended in blocking buffer and incubated at room temperature for 1.5 hours and then transferred to 4°C for overnight incubation. The following day the sections were washed 3 × 10 minutes with PBS. Fluorophore-tagged secondary antibodies were resuspended in blocking buffer, and then added to sections for incubation at room temperature for 2 hours. Finally, sections were washed 3 × 10 minutes in PBS and mounted with ProLong Gold antifade reagent with DAPI and imaged on the Zeiss (White Plains, NY) LSM 880 microscope. H&E, AB/PAS, CD3, and F4/80 staining were performed by the Vanderbilt University Medical Center Translational Pathology Shared Resource core and images were acquired on the Nikon (Tokyo, Japan) AZ 100 M equipped with a Nikon DS-Ri1 color camera.

Fluorescence In Situ Hybridization

Fluorescence in situ hybridization was performed as previously described.[24] Paraffin sections were dewaxed and washed in 95% ethanol. The sections then were incubated with 250 μg of Cy3-conjugated EUB 338 (sequence derived from EU622773 bacteria ribosomal RNA) oligo (5′-GCTGCCTCCCGTAGGAGT-3′, bp 337–354 in bacteria EU622773) in 50 μL of hybridization buffer (20 mmol/L TRIS-HCl [pH 7.4], 0.9 mol/L NaCl, 0.1% sodium dodecyl sulfate) at 50°C overnight. The sections were rinsed in wash buffer (20 mmol/L TRIS-HCl [pH 7.4], 0.9 mol/L NaCl), washed at 50°C for 20 minutes, and counterstained with DAPI. Co-immunostaining with anti-Muc2 antibody was performed at 4°C without antigen retrieval and mounted in prolong Gold antifade.

NKCC1-DFX Mice

The generation of NKCC1-DFX mice was described in a recent publication.[15] All procedures with mice were approved by the Vanderbilt University Medical Center Animal Care and Use Committee.

Fecal Water Content Quantification

Fresh stools were collected onto preweighed small square pieces of aluminum foil (boats), weighed immediately, and placed in a glass Petri dish. After collection and determination of fresh weights, the samples were incubated in an oven at 110°C for 24 hours. Aluminum boats with dried stools then were reweighed, and fecal water was determined as the fraction of total mass lost upon desiccation. Water content was calculated as follows: (fresh weight – dry weight)/dry weight.

Measurement of Intestinal Transit

Carmine (C1022; Sigma-Aldrich) prepared at 6% overnight in 0.5% methylcellulose (274429; Sigma-Aldrich) in filtered 0.09% NaCl and stored at 4°C before use. Solution was warmed up to room temperature before gavage. Nine- to 10-week-old mice of the 3 genotypes were fed with 300 μL carmine solution through 20-ga × 30-mm plastic feeding tubes (Instech Laboratories, Inc, Plymouth Meeting, PA) placed on a 1-mL syringe and individually placed in cages without bedding and water for the remaining of the experiment. Times of gavage and deposition of first red fecal pellets were recorded before the mice were returned to their home cages.

Transmission Electron Microscopy

Freshly excised colonic tissue from mice was washed quickly in 0.1 mol/L cacodylate buffer. Samples then were fixed in 2.5% glutaraldehyde (in 0.1 mol/L sodium phosphate, pH 7.4, containing 0.1 mol/L Na-cacodylate) for 30 minutes at room temperature, followed by overnight postfixation at 4°C. After several washes, samples were treated with 1% osmium tetroxide for 1 hour and dehydrated through serial ethanol solutions (30%, 50%, 70%, 95%, and 100%). Samples then were incubated with propylene oxide followed by removal of ethanol from the samples before infiltration with and embedding in EPON 812 resin. Ultrathin (70- to 80-nm thick) sections were cut and collected on 300-mesh copper grids. Sections were stained with 2% uranyl acetate, followed by Reynold's lead citrate, and imaged using a Philips/FEI (Hillsboro, OR) T-12 Tecnai electron microscope.

Preparation of C rodentium

The open reading frame of the firefly luciferase gene was excised from pGL3 basic (Promega, Madison, WI) using *Nco*I + *Bam*HI and ligated into the bacterial expression vector pET28a (EMD Millipore, Burlington, MA). *C rodentium* (ATCC 51459) were grown overnight at 37°C in Luria Broth medium. The next day, 500 μL of the culture was added to 50 mL LB and grown to an optical density at 600 nm of 0.3. The cells then were pelleted at 8000 rpm for 5 minutes and the pellet was resuspended in 5 mL ice-cold $CaCl_2$ (30 mmol/L) solution. Aliquots of 1 mL then were spun in 1.5-mL Eppendorf tubes, and the pellets were resuspended in 500 μL ice-cold $CaCl_2$ (30 mmol/L) solution and subdivided into 50-uL aliquots. The luciferase_pET28a vector then was transformed into competent *Citrobacter* cells and plated on a kanamycin-resistant plate. Kanamycin-resistant *Citrobacter* colonies then were picked and grown in 4 mL LB medium with kanamycin and aliquoted at -80°C in LB containing 16.7% glycerol.

Clearance of C rodentium in Mixed C57:DBA Mice

Mice were infected by oral gavage with 0.2 mL of an overnight culture of LB containing approximately 2×10^9 colony forming units of a kanamycin-resistant *C rodentium* DBS100 (ICC180). Fresh stools were collected at the indicated time points and transferred to a preweighed 1.5-mL Eppendorf tube containing 100 μL Hank's balanced salt solution HBSS containing Ca^{2+} and Mg^{2+}). The weight of the fresh stool was determined by subtracting the weight of the stool-containing Eppendorf tube from the pre-tare value. The pellets then were resuspended at a ratio of 0.1 g of pellet per 1 mL $HBSS^{2+}$. Pellets were left to soften in $HBSS^{2+}$ for 20 minutes, and then dispersed by pipetting up and down a few times through a 1-mL pipette tip. The slurry then was passed through a 70-μm Corning cell strainer (cat. 352350; Thermo Fisher Scientific) and collected. To assess titers, 50 μL of the filtered slurries was plated on LB agar plates containing kanamycin and incubated at 37°C overnight. The number of colonies on the plates was counted the next day.

Serum Cytokine Measurement

Mice were anesthetized with isoflurane and blood was collected via cardiac puncture. Blood then was centrifuged in 1.5-mL Eppendorf tubes at 6000 rpm for 10 minutes. Serum was collected and saved at -80°C until used. Inflammatory cytokines in serum were detected using a 6-Plex Th17 enzyme-linked immunosorbent assay panel (Bio-Rad), according to the manufacturer's recommendation.

Isolation of Intestinal Epithelial Cells

Intestinal epithelial cells were obtained from freshly isolated colons. Colons were flushed and washed multiple times with sterile ice-cold $HBSS^{2-}$ (HBSS without Ca^{2+} and Mg^{2+}). Colons then were opened longitudinally and washed thoroughly in $HBSS^{2-}$. They then were incubated in 10 mL Gentle Cell Dissociation Reagent (Stemcell Technologies, Cambridge, MA) and rotated at 4°C for 30 minutes. Tissue then was removed and cells were washed in ice-cold $HBSS^{2-}$ and passed through a 70-μm filter. The cells then were centrifuged at 900 $\times$ *g* for 4 minutes at 4°C, washed in $HBSS^{2-}$, and spun for another 4 minutes at 900 $\times$ *g*. Cell pellets were finally lysed in 1 mL TRIzol and RNA was extracted according to the manufacturer's protocol.

Quantitative Reverse-Transcription Polymerase Chain Reaction

RNA (2–5 μg) was reverse-transcribed using Superscript III (Stratagene, La Jolla, CA) according to the manufacturer's protocol. The complementary DNA then was diluted 1:4 and quantitative polymerase chain reaction (PCR) was performed on a ABI 7000 StepOnePlus real time PCR machine (Applied Biosystem, Foster City, CA). The sequences of the primers used were as follows: Hes1-forward: 5'-TCAACACGACACCGGACAAAC-3'; Hes1-reverse 5'-ATGCCGGGAGCTATCTTTCTT-3', Gfi1 forward: 5'-AGAAGGCGCACAGCTATCAC-3', Gfi1 reverse: 5'-GGCTCCATTTTCGACTCGC-3', Spdef forward: 5'-ATGGACAGAACACCAGTACCG-3'; Spdef reverse: 5'-AGGCGCAGTAGTGAAGGGT-3'; Klf4 forward 5'-AGGAACTCTCTCAC ATGAAGCG-3'; Klf4 reverse: 5'-GGTCGTTGAACTCCTCGGTC-3'; and TFF3 forward: 5'-TTGCTGGGTCCTCTGGGATAG-3'; TFF3 reverse: 5'-TACACTGCTCCGATGTGACAG-3'. Quantitative PCR reactions contained 12.5 μL SYBR Green PCR master mix (Applied Biosystems), 1 μL of each primer (1 μmol/L), 9.5 μL water, and 1 μL complementary DNA. Data were expressed relative to glyceraldehyde-3-phosphate dehydrogenase expression. The primers for this housekeeping gene were as follows: glyceraldehyde-3-phosphate dehydrogenase forward: 5'-AGGTCGGTGTGAACGGATTTG-3' and glyceraldehyde-3-phosphate dehydrogenase reverse: 5'-GGGGTCGTTGATGGCAACA-3'. The PCR cycling conditions used were an initial denaturation step at 95°C for 5 minutes, followed by denaturation at 95°C for 30 seconds, annealing for 30 seconds at 60°C, and extension at 72°C for 30 seconds. These short steps were repeated or cycled 40 times. The melting curve analysis confirmed the presence of only 1 pick for each primer set.

References

1. Geck P, Pietrzyk C, Burckhardt B-C, Pfeiffer B, Heinz E. Electrically silent cotransport of Na^+, K^+ and Cl^- in Ehrlich cells. Biochim Biophys Acta 1980;600:432–447.
2. Plotkin MD, Snyder EY, Hebert SC, Delpire E. Expression of the Na-K-2Cl cotransporter is developmentally regulated in postnatal rat brains: a possible mechanism underlying GABA's excitatory role in immature brain. J Neurobiol 1997;33:781–795.
3. Dzhala VI, Talos DM, Sdrulla DA, Brumback AC, Mathews GC, Benke TA, Delpire E, Jensen FE, Staley KJ. NKCC1 transporter facilitates seizures in the developing brain. Nat Med 2005;11:1205–1213.
4. Alvarez-Leefmans FJ, Gamiño SM, Giraldez F, Nogueron I. Intracellular chloride regulation in amphibian dorsal root ganglion neurons studied with ion-selective microelectrodes. J Physiol (Lond) 1988;406:225–246.
5. Sung K-W, Kirby M, McDonald MP, Lovinger DM, Delpire E. Abnormal $GABA_A$-receptor mediated currents in dorsal root ganglion neurons isolated from Na-K-2Cl cotransporter null mice. J Neurosci 2000;20:7531–7538.
6. Akar F, Jiang G, Paul RJ, O'Neill WC. Contractile regulation of the Na(+)-K(+)-2Cl(-) cotransporter in vascular smooth muscle. Am J Physiol Cell Physiol 2001; 281:C579–C584.
7. Koltsova SV, Kotelevtsev SV, Tremblay J, Hamet P, Orlov SN. Excitation-contraction coupling in resistance mesenteric arteries: evidence for NKCC1-mediated pathway. Biochem Biophys Res Commun 2009; 379:1080–1183.
8. He X, Tse CM, Donowitz M, Alper SL, Gabriel SE, Baum BJ. Polarized distribution of key membrane transport proteins in the rat submandibular gland. Pflugers Arch 1997;433:260–268.
9. McDaniel N, Lytle C. Parietal cells express high levels of Na-K-2Cl cotransporter on migrating into the gastric gland neck. Am J Physiol 1999;276:G1273–G1278.

10. Cui CY, Childress V, Piao Y, Michel M, Johnson AA, Kunisada M, Ko MS, Kaestner KH, Marmorstein AD, Schlessinger D. Forkhead transcription factor FoxA1 regulates sweat secretion through Bestrophin 2 anion channel and Na-K-Cl cotransporter 1. Proc Natl Acad Sci U S A 2012;109:1199–1203.
11. Flemmer AW, Gimenez I, Dowd BF, Darman RB, Forbush B. Activation of the Na-K-Cl cotransporter NKCC1 detected with a phospho-specific antibody. J Biol Chem 2002;277:37551–37558.
12. Flores-Delgado G, Lytle C, Quinton PM. Site of fluid secretion in small airways. Am J Respir Cell Mol Biol 2016;54:312–318.
13. Delpire E, Wolfe L, Flores B, Koumangoye R, Schornak CC, Omer S, Pusey B, Lau C, Markello T, Adams DR. A patient with multisystem dysfunction carries a truncation mutation in human *SLC12A2*, the gene encoding the Na-K-2Cl cotransporter, NKCC1. Cold Spring Harb Mol Case Studies 2016;2:a001289.
14. Macnamara EF, Koehler AE, D'Souza P, Estwick T, Lee P, Vezina G, Diseaes Network Undiagnosed, Fauni H, Braddock SR, Torti E, Holt JM, Sharma P, Malicdan MCV, Tifft CJ. Kilquist syndrome: a novel syndromic hearing loss disorder caused by homozygous deletion of SLC12A2. Hum Mutat 2019;40:532–538.
15. Koumangoye R, Omer S, Delpire E. Mistargeting of a truncated Na-K-2Cl cotransporter in epithelial cells. Am J Physiol Cell Physiol 2018;315:C258–C276.
16. Delpire E, Lu J, England R, Dull C, Thorne T. Deafness and imbalance associated with inactivation of the secretory Na-K-2Cl co-transporter. Nat Genet 1999; 22:192–195.
17. Flagella M, Clarke LL, Miller ML, Erway LC, Giannella RA, Andringa A, Gawenis LR, Kramer J, Duffy JJ, Doetschman T, Lorenz JN, Yamoah EN, Cardell EL, Shull GE. Mice lacking the basolateral Na-K-2Cl cotransporter have impaired epithelial chloride secretion and are profoundly deaf. J Biol Chem 1999; 274:26946–26955.
18. Dixon MJ, Gazzard J, Chaudhry SS, Sampson N, Schulte BA, Steel KP. Mutation of the Na-K-Cl co-transporter gene Slc12a2 results in deafness in mice. Hum Mol Genet 1999;8:1579–1584.
19. Pace AJ, Lee E, Athirakul K, Coffman TM, O'Brien DA, Koller BH. Failure of spermatogenesis in mouse lines deficient in the Na^+-K^+-$2Cl^-$ cotransporter. J Clin Invest 2000;105:441–450.
20. Wouters M, De Laet A, Ver Donck L, Delpire E, van Bogaert PP, Timmermans JP, de Kerchove d'Exaerde A, Smans K, Vanderwinden JM. Subtractive hybridization unravels a role for the ion co-transporter NKCC1 in the murine intestinal pacemaker. Am J Physiol Gastrointest Liver Physiol 2006;290:G1219–G1227.
21. Zhu MH, Sung TS, Kurahashi M, O'Kane LE, O'Driscoll K, Koh SD, Sanders KM. Na^+-K^+-Cl^- cotransporter (NKCC) maintains the chloride gradient to sustain pacemaker activity in interstitial cells of Cajal. Am J Physiol Gastrointest Liver Physiol 2016; 311:G1037–G1046.
22. Delpire E, Gagnon KB. Na^+-K^+-$2Cl^-$ cotransporter (NKCC) physiological function in nonpolarized cells and transporting epithelia. Compr Physiol 2018;8:871–901.
23. Pelaseyed T, Bergström JH, Gustafsson JK, Ermund A, Birchenough GM, Schütte A, van der Post S, Svensson F, Rodríguez-Piñeiro AM, Nyström EE, Wising C, Johansson ME, Hansson GC. The mucus and mucins of the goblet cells and enterocytes provide the first defense line of the gastrointestinal tract and interact with the immune system. Immunol Rev 2014; 260:8–20.
24. Johansson ME, Phillipson M, Petersson J, Velcich A, Holm L, Hansson GC. The inner of the two Muc2 mucin-dependent mucus layers in colon is devoid of bacteria. Proc Natl Acad Sci U S A 2008;105:15064–15069.
25. Leverkoehne I, Gruber AD. The murine mCLCA3 (alias gob-5) protein is located in the mucin granule membranes of intestinal, respiratory, and uterine goblet cells. J Histochem Cytochem 2002;50:829–838.
26. Delpire E, Gagnon KB. Water homeostasis and cell volume maintenance and regulation. Curr Top Membr 2018; 81:3–52.
27. Wu Q, Delpire E, Hebert SC, Strange K. Functional demonstration of Na-K-2Cl cotransporter activity in isolated, polarized choroid plexus cells. Am J Physiol Cell Physiol 1998;275:C1565–C1572.
28. Gregoriades JMC, Madaris A, Alvarez FJ, Alvarez-Leefmans FJ. Genetic and pharmacologic inactivation of apical NKCC1 in choroid plexus epithelial cells reveals the physiological function of the cotransporter. Am J Physiol Cell Physiol 2019;316:C525–C544.
29. McCauley HA, Guasch G. Three cheers for the goblet cell: maintaining homeostasis in mucosal epithelia. Trends Mol Med 2015;21:492–503.
30. Wong WM, Poulsom R, Wright NA. Trefoil peptides. Gut 1999;44:890–895.
31. Walker NM, Flagella M, Gawenis LR, Shull GE, Clarke LL. An alternate pathway of cAMP-stimulated Cl secretion across the NKCC1-null murine duodenum. Gastroenterology 2002;123:531–541.
32. Hoegger MJ, Fischer AJ, McMenimen JD, Ostedgaard LS, Tucker AJ, Awadalla MA, Moninger TO, Michalski AS, Hoffman EA, Zabner J, Stoltz DA, Welsh MJ. Impaired mucus detachment disrupts mucociliary transport in a piglet model of cystic fibrosis. Science 2014;345:818–822.
33. Van der Sluis M, De Koning BA, De Bruijn AC, Velcich A, Meijerink JP, Van Goudoever JB, Büller HA, D, J, Van Seuningen I, Renes IB, Einerhand AW. Muc2-deficient mice spontaneously develop colitis, indicating that MUC2 is critical for colonic protection. Gastroenterology 2006;131:117–129.
34. Garcia MA, Yang N, Quinton PM. Normal mouse intestinal mucus release requires cystic fibrosis transmembrane regulator-dependent bicarbonate secretion. J Clin Invest 2009;119:2613–2622.
35. Gustafsson JK, Ermund A, Ambort D, Johansson ME, Nilsson HE, Thorell K, Hebert H, Sjövall H, Hansson GC. Bicarbonate and functional CFTR

channel are required for proper mucin secretion and link cystic fibrosis with its mucus phenotype. J Exp Med 2012;209:1263–1272.
36. Crepin VF, Collins JW, Habibzay M, Frankel G. Citrobacter rodentium mouse model of bacterial infection. Nat Protoc 2016;11:1851–1876.
37. Parameswaran N, Patial S. Tumor necrosis factor-α signaling in macrophages. Crit Rev Eukaryot Gene Expr 2010;20:87–103.
38. Feldmann M, Brennan FM, Elliott M, Katsikis P, Maini RN. TNF alpha as a therapeutic target in rheumatoid arthritis. Circ Shock 1994;43:179–184.
39. Maini RN, Elliott MJ, Brennan FM, Feldmann M. Beneficial effects of tumour necrosis factor-alpha (TNF-alpha) blockade in rheumatoid arthritis (RA). Clin Exp Immunol 1995;101:207–212.
40. Feldmann M, Maini RN. Anti-TNF alpha therapy of rheumatoid arthritis: what have we learned? Annu Rev Immunol 2001;19:163–196.
41. Monaco C, Nanchahal J, Taylor P, Feldmann M. Anti-TNF therapy: past, present and future. Int Immunol 2015;27:55–62.
42. Giuffrida P, Cococcia S, Delliponti M, Lenti MV, Di Sabatino A. Controlling gut inflammation by restoring anti-inflammatory pathways in inflammatory bowel disease. Cells 2019;8, pii: E397.
43. Tokuda S, Furuse M. Claudin-2 knockout by TALEN-mediated gene targeting in MDCK cells: claudin-2 independently determines the leaky property of tight junctions in MDCK cells. PLoS One 2015;10:e0119869.
44. Zhang Y, Viennois E, Xiao B, Baker MT, Yang S, Okoro I, Yan Y. Knockout of Ste20-like proline/alanine-rich kinase (SPAK) attenuates intestinal inflammation in mice. Am J Pathol 2013;182:1617–1628.
45. Gagnon KB, Delpire E. Molecular physiology of SPAK and OSR1: two Ste20-related protein kinases regulating ion transport. Physiol Rev 2012;92:1577–1617.
46. Schnermann J, Huang Y, Mizel D. Fluid reabsorption in proximal convoluted tubules of mice with gene deletions of claudin-2 and/or aquaporin1. Am J Physiol Renal Physiol 2013;305:F1352–F1364.
47. Matsumoto K, Imasato M, Yamazaki Y, Tanaka H, Watanabe M, Eguchi H, Nagano H, Hikita H, Tatsumi T, Takehara T, Tamura A, Tsukita S. Claudin 2 deficiency reduces bile flow and increases susceptibility to cholesterol gallstone disease in mice. Gastroenterology 2014;147:1134–1145.
48. Tsai PY, Zhang B, He WQ, Zha JM, Odenwald MA, Singh G, Tamura A, Shen L, Sailer A, Yeruva S, Kuo WT, Fu YX, Tsukita S, Turner JR. IL-22 upregulates epithelial claudin-2 to drive diarrhea and enteric pathogen clearance. Cell Host Microbe 2017;21:671–681.

Received July 20, 2019. Accepted October 15, 2019.

Correspondence
Address correspondence to: Eric Delpire, PhD, Department of Anesthesiology, Vanderbilt University School of Medicine, T-4202 Medical Center North, 1161 21st Avenue South, Nashville, Tennessee 37232-2520. e-mail: eric.delpire@vanderbilt.edu; fax: (615) 343-3916.

Acknowledgments
The authors wish to acknowledge Lynne Wolf and Dr William A. Ghal from the National Institutes of Health Undiagnosed Diseases Program (Bethesda, MD) for providing a fragment of patient UDP-2780 colon. The authors also wish to thank Ghali Abdelmessih for his assistance in managing our Na^+-K^+-$2Cl^-$ cotransporter mouse colony and for genotyping.

Author contributions
Rainelli Koumangoye and Eric Delpire designed the research studies; Rainelli Koumangoye, Salma Omer, and Eric Delpire conducted experiments and acquired and analyzed data; Mustafa H. Kabeer provided the patient colon sample to the National Institutes of Health undiagnosed diseases program, completed the clinical and pathology reports, and provided expertise; and all authors contributed to manuscript writing, editing, and approval of the final version.

Conflicts of interest
The authors disclose no conflicts.

Funding
This work was supported by National Institutes of Health grants GM118944 and DK093501 (E.D.), and in part by Clinical and Translational Science Awards award UL1TR002243 from the National Center for Advancing Translational Sciences (R.K.). The content is solely the responsibility of the authors and does not necessarily represent the official views of the National Center for Advancing Translational Sciences or the National Institutes of Health. Electron microscopy and confocal imaging was performed in part through the use of the Vanderbilt University Medical Center Cell Imaging Shared Resource, which is supported by National Institutes of Health grants CA68485, DK20593, DK58404, DK59637, and EY08126. Tissue sectioning, H&E, AB/PAS, and CD3 staining were performed by the Vanderbilt University Medical Center VUMC Translational Pathology Shared Resource, which is supported by National Institutes of Health grants CA68485, DK20593, DK58404, and HD15052.